

Polar lows over the Nordic and Labrador Seas: Synoptic circulation patterns and associations with North Atlantic-Europe wintertime weather regimes

Paul-Etienne Mallet,¹ Chantal Claud,¹ Christophe Cassou,² Gunnar Noer,³ and Kunihiko Kodera⁴

Received 11 June 2012; revised 29 January 2013; accepted 31 January 2013; published 16 March 2013.

[1] Polar Lows (PLs) are intense meso-cyclones forming in winter at high latitudes over open water. Using several datasets of PLs over the North Atlantic, the synoptic environment conducive to their development is determined. The 500 hPa geopotential height, the difference between the sea surface temperature and the 500 hPa air temperature, the near-surface wind and air temperature, and the 300 hPa potential vorticity present significant anomaly patterns over large areas centered over PL genesis zones, suggesting cold air outbreaks and stratospheric intrusions. PLs develop within a northerly flow in the Norwegian Sea, a northeasterly flow in the Barents Sea and a westerly flow in the Labrador Sea. PLs form after a certain build-up, the outbreak day being marked by strong winds and PV intensification. The relationship between PLs and daily weather regimes over North Atlantic-Europe is then investigated. Regimes have a typical lifetime of 8–10 days, similar to the large-scale anomalies associated with PLs. Over the Norwegian and Barents seas from 1999 to 2011, 37% of PLs are observed during the Atlantic Ridge regime (AR) and 28% in the negative phase regime of the North Atlantic Oscillation (NAO), whereas PL probability of occurrence is reduced by half for the positive phase of NAO and the Scandinavian blocking (SB) regimes. Over the Labrador Sea, most PLs occur during NAO+ while they are almost absent during NAO-. Demonstrating the temporal variation of key factors based on an updated dataset and relating PLs to weather regimes will introduce novel and important elements in PL forecasting methodology.

Citation: Mallet, P.-E., C. Claud, C. Cassou, G. Noer and K. Kodera (2013), Polar lows over the Nordic and Labrador Seas: Synoptic circulation patterns and associations with North Atlantic-Europe wintertime weather regimes, *J. Geophys. Res. Atmos.*, 118, 2455–2472, doi:10.1002/jgrd.50246.

1. Introduction

[2] Polar lows (PLs) are high-latitude intense maritime cyclones, characterized by their small horizontal scale (between 200 and 1000 km), their short lifetime (one to two days), and surface winds which can exceed 30 m s^{-1} [Heinemann and Claud, 1997]. There are other severe conditions associated with PLs, such as large-amplitude ocean waves [e.g., Claud *et al.*, 1993] and heavy snow showers with severely limited visibility [Harrold and Browning, 1969].

Therefore, they remain difficult to accurately forecast. Recent investigations indicate that PLs may contribute to ocean-atmosphere coupling by increasing depth, frequency, and area of deep convection in the Nordic seas, which in turn lead to modify oceanic circulation [Saetra *et al.*, 2008; Condron and Renfrew, 2013]. PLs may form throughout the year in the Southern Hemisphere around the Antarctic or near “South America” or Australia [e.g., Carleton and Carpenter, 1990; Auer, 1986; Zick, 1994; McMurdie *et al.*, 1997]; however, they are a wintertime phenomenon in the Northern Hemisphere. There, they occur mainly in the Norwegian and Barents Seas [Rasmussen and Turner, 2003] but are also observed in other open sea areas, like the Labrador Sea and the Greenland Sea [Rasmussen, 1990; Rasmussen *et al.*, 1996; Moore *et al.*, 1996], and occasionally to the north of the United Kingdom [e.g., Hewson *et al.*, 2000]. Additional PL genesis regions are the Okhotsk Sea and the Japan Sea [Ninomiya, 1989; Ninomiya *et al.*, 1990; Yanase *et al.*, 2004; Mitnik *et al.*, 2011], the far Northeast Pacific and the Bering Strait [Businger, 1987; Businger and Baik, 1991; Douglas *et al.*, 1991], and other higher latitude areas where and when sea ice is absent, like Baffin Bay and the Beaufort Sea [Parker, 1989; Rasmussen *et al.*, 1993]. With the recent rapid

All supporting information may be found in the online version of this article.

¹Laboratoire de Météorologie Dynamique/IPSL, CNRS, Ecole Polytechnique, Palaiseau, France.

²CERFACS/CNRS, Climate Modeling and Global Change Team, Toulouse, France.

³The Norwegian Meteorological Institute, Tromsøe, Norway.

⁴Solar-Terrestrial Environment Laboratory, Nagoya University, Japan.

Corresponding author: P.-E. Mallet, Laboratoire de Météorologie Dynamique/IPSL, CNRS, Ecole Polytechnique, Palaiseau, France. (pemallet@lmd.polytechnique.fr)

decrease in sea-ice extent over the Pacific sector of the Arctic during intermediate seasons, the Chukchi Sea might also see more PL developments especially in the fall season [e.g., *Inoue et al.*, 2010].

[3] The relatively small-scale and short life time of PLs means they are generally not well represented in model outputs and meteorological reanalysis data sets, as shown by *Condron et al.* [2006] for the ERA-40 reanalysis. Nevertheless, reanalysis data are a valuable tool to study their typical synoptic or large-scale environment [e.g., *Claud et al.*, 2007, 2009a, 2009b; *Kolstad*, 2011]. Because PLs generally form when cold air from polar latitudes is transported from ice-covered sea or land equatorward over relatively warm open sea, where large vertical fluxes of heat and moisture favor more intense mesocyclonic development, the primary tool for their forecasting is an assessment of the associated synoptic-scale flow pattern. This can be determined from cataloguing recurrent patterns in the atmospheric or oceanic large-scale circulation variability associated with PL development. However, PL formation does not result from a single condition but rather from a set of conditions [*Rasmussen and Turner*, 2003] that lead to different types of PLs depending on the combination of those forcing mechanisms.

[4] Studies concerning the occurrence of PLs in and around the Nordic Seas, and the large-scale environments in which they form, have been conducted over many years [e.g., *Forbes and Lottes*, 1985; *Businger*, 1985; *Ese et al.*, 1988 for the pioneer works]. These authors found that the synoptic-scale environment plays a considerable role in determining which incipient vortices continue to develop. They all found significant negative height and temperature anomalies in the 500 hPa synoptic-scale fields on days when PLs occurred, indicating strong positive vorticity advection and low static stability, together with a barotropic structure of the atmosphere over these storms. *Businger* [1985] also examined the evolution of the anomalies over the key day -5 to key day $+5$ windows, with the key day 0 being defined as the date on which PLs appear to be mature. This author also showed a tendency for in situ development of anomaly features prior to the key day. Moreover, he observed that the negative anomalies gradually migrate southward following the key day, reaching their lowest values 1 day after the key day and weakening rapidly thereafter.

[5] More recently, the large-scale atmospheric circulation during PL events over the Nordic Seas has been investigated based on a PL data set derived purely from satellite observations for the years 2004–2005 [*Blechschmidt et al.*, 2009]. These authors distinguished four different types of PLs and their characteristic large-scale circulation patterns of sea level pressure and 500 hPa geopotential height, and the differences between the ocean skin temperature and the 500 hPa temperature. A long-term climatology (1948–2006) of PLs for the sub-Arctic region of the North Atlantic [*Zahn and von Storch*, 2008] has been built through a dynamical downscaling of NCEP/NCAR reanalyses [*Kalnay et al.*, 1996]. Through a Canonical Correlation Analysis [*von Storch and Zwiers*, 1999], these authors showed characteristic meridional mean flow regimes, which favor cold air outbreaks and upper troughs. A global climatology of favorable conditions for PLs has been presented by *Kolstad* [2011], based on satellite observations of PLs, and quantifies the

respective influences of low-level static stability and upper level forcing on PL development. According to this author, the first parameter places important constraints on where PLs can form, while the second parameter determines whether or not they will form.

[6] In a previous paper, *Claud et al.* [2007] described the associations between dominant patterns of low-frequency variability in the atmospheric circulation, or teleconnections, and PLs over the Nordic Seas during winter. They found that the key variables determining PL formation may be strongly influenced by the North Atlantic Oscillation (NAO), and the Scandinavia Pattern, with spatial and temporal contrasts. These teleconnections traditionally are determined either using linear techniques such as eigenmodes decomposition or one-point correlation [*Wallace and Gutzler*, 1981; *Blackmon et al.*, 1984]. This approach is based on the hypothesis that atmospheric oscillations occur around a defined mean state. An alternative point of view considers that the atmosphere evolves between several preferential states, the so-called weather regimes (hereafter WRs or simply “regimes”). WRs can be seen as peaks in the density function of the climate phase space. In mid-latitudes, they correspond to preferred and/or recurrent quasi-stationary atmospheric circulation patterns produced by the interaction between planetary-scale and synoptic-scale atmospheric waves [*Ghil and Robertson*, 2002]. Unlike in the linear approach, WRs do not come in pairs with the same anomalous spatial structures of opposite polarity; rather, they have a typical 8–10 day persistence, are spatially well defined, are limited in number, and have the advantage of representing a large part of the seasonal atmospheric variability [*Vautard*, 1990; *Feldstein*, 2000]. During boreal winter (November to March), four weather regimes are defined in the literature for the North Atlantic–Europe sector: two associated with the alternation in strength and latitudinal position of the zonal flow, corresponding to the negative and positive phases of the NAO (hereafter referred to as NAO+ and NAO– regimes, respectively), and two corresponding to pronounced meridional flow patterns such as the Atlantic Ridge (AR) and Scandinavian Blocking (SB) regimes.

[7] To the knowledge of the authors, there has been no attempt so far to relate the occurrence of PLs to WRs; hence, the present study. Moreover, the temporal aspect of pre-development conditions is observed frequently at the forecast center in northern Norway, but for lack of firm results from more recent data, it has not been implemented in PL forecasting methodology. The lack of understanding of the time dependency of critical factors in the formation of PLs is a main source of false or erratic forecasts and accounts for many “false alarms” of PL development. Similarly, the importance of upper level forcing in cyclogenesis has received little attention in previous studies and is a focus of this study. Two new multiyear (1999–2011) PL databases [*Noer et al.*, 2011; *Kolstad*, 2011] are consistent with the definition of PLs given by *Heinemann and Claud* [1997] and are based on recent observations with modern remote sensing tools; in addition, recent reanalyses have a higher spatial resolution; hence, these aspects can now be investigated with a higher degree of precision than in previous studies.

[8] The objectives of this study are twofold: (1) to re-examine the statistical relationships between the large-scale environment

and PL activity in the Norwegian Sea, emphasizing not only conditions at the time of formation but also the pre-development conditions; and (2) to investigate the associations between North Atlantic WRs and PL activity over the Nordic and Labrador Seas. The achievement of both objectives will contribute to an improved forecasting of PLs on time scales ranging from daily to weekly.

[9] In the next section, we present the data and methods. Then the synoptic environment for PLs observed in several formation areas is investigated, in order to characterize the typical conditions of their formation and their evolution. In section 4, the associations between PL formation and WRs are investigated for the Norwegian and Barents Seas contrasted with the Labrador Sea. The results of the study are summarized in section 5.

2. Data and Methodology

2.1. PL Datasets

[10] This study is based on two recent PL datasets, the first covering the eastern sector of the North Atlantic [Noer *et al.*, 2011] and the other one covering the western sector [Kolstad, 2011]. To increase the statistical robustness and as a check on the temporal stability of the results, we also use four older and less homogeneous databases which are based on various observation methods (ground measurements only, or coupled with satellites) and PLs selection criteria. The main characteristics of the PL inventories are shown in Table 1, with their spatial distributions given schematically in Figure 1.

[11] The dataset by Noer *et al.* [2011] consists of 134 PL events over the Norwegian and Barents seas from 1999 to 2011, based on subjective observations by trained forecasters from the Norwegian Meteorological Institute, of model fields and satellite data. The latter includes infrared imagery from the National Oceanic and Atmospheric Administration (NOAA) Advanced Very High Resolution Radiometer (AVHRR), scatterometer winds from ASCAT (Advanced Scatterometer), and QuikSCAT (Quick Scatterometer), and also considers gale-force wind criteria (depressions with weak surface winds are eliminated). The annually updated list can be found online at <http://met.no/Forsking/Publikasjoner/>. The data set by Kolstad [2011] consists of 19 PLs that formed west of 30°W over the 2000–2009 period. This inventory was based on AVHRR manual inspection. The PL formation times and locations were then deduced from ERA-Interim (ERA-I) data. A gale-force wind criterion was not directly retained, but cases for which the QuikSCAT data did not show any indication of cyclonic circulation and strong wind speed were excluded.

[12] Concerning the additional datasets, Wilhelmsen [1985] listed 33 PLs over the period 1978–1982, from inspection of

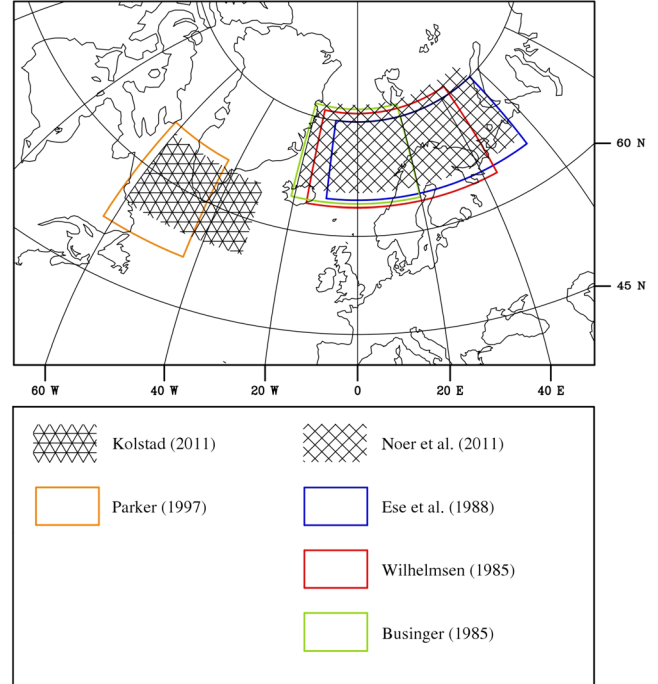


Figure 1. Approximate area for each PL dataset (see text and Table 1 for more details).

meteorological weather maps, synoptic observations from ships and coastal stations, and a few satellite images. Only PLs having gale-force winds or stronger were considered. As mentioned earlier, Businger [1985] formed two lists of PLs covering the 1971 to 1983 period: the first consisting of 42 cases obtained on the basis of synoptic and surface data and the second of 10 cases based on the inspection of infrared satellite images. The Ese *et al.* [1988] list, based on surface and, when available, satellite observations for the period 1971–1983, contains 74 PLs. Before March 1982, only lows that affected the Norwegian coast are considered. Note that out of these three data sets, only that by Wilhelmsen includes a wind speed criterion. In addition, these data sets partially overlap and include the same cases. For example, Businger and Ese have 34 identical cases; Wilhelmsen and Ese, 24 identical cases. Finally, we considered an inventory of 121 PLs that formed over the period 1977–1994 near the Canadian coast [Parker, 1997]. This list is based on the inspection of polar orbiting satellite imagery and, when possible, GOES (NOAA Geostationary satellites) imagery. Cases from this list extend over a very large area. We retained the 93 PLs that formed in the Labrador Sea, to the east of 62°W and between 52°N and 66°N.

Table 1. Characterization of PL Databases Used in This Study

	Period	Approximate Area	Total PL Number	PL Number for Nov.-Mar.	Wind Criteria
Noer <i>et al.</i> [2011]	1999–2011	20°W–55°E/65°N–77°N	156	134	Gale force
Ese <i>et al.</i> [1988]	1971–1983	10°W–55°E/65°N–75°N	74	45	/
Wilhelmsen [1985]	1978–1982	16°W–44°E/64°N–76°N	33	27	Gale force
Businger [1985]	1971–1983	20°W–20°E/65°N–75°N	52	35	/
Kolstad [2011]	2000–2009	60°W–30°W/55°N–65°N	63	19	Near gale force wind speed
Parker [1997]	1977–1994	62°W–43°W/52°N–66°N	121	72	/

[13] When large-scale conditions are favorable, PLs generally form in clusters of multiple low-pressure centers [e.g., *Noer et al.*, 2011]. However, an individual vortex/system is frequently represented in these datasets as a unique case, by date (and sometimes position) of its first identification as a mature system. Because this study focuses on the synoptic conditions leading to the formation of PLs, an event corresponding to an outbreak of several PLs is not given more weight than a single meso-cyclogenesis event.

2.2. Reanalyses

[14] Daily mean fields from the ERA-Interim (ERA-I) and the NCEP/NCAR Reanalysis are utilized. ERA-I is the latest European Center for Medium-range Weather Forecasts (ECMWF) global atmospheric reanalysis [*Dee et al.*, 2011]. It covers the period 1979 to the present with a 0.75° latitude 0.75° longitude grid resolution and has 37 vertical levels.

[15] For PL cases prior to 1979 and for determining daily WR, we used the NCEP/NCAR Reanalysis with an approximate 2° grid resolution and which covers the period from 1948 to the present [*Kalnay et al.*, 1996].

[16] *Noer and Ovhed* [2003] identified several variables designating key factors in the development and forecasting of PLs. The wind at 925 hPa is considered an indicator of cold air outbreak. The potential for deep convection over an area can be determined from the geopotential height at 500 hPa (Z500). Because thermodynamical fluxes play an important role in PL intensification, the sea surface temperature (SST) is highly relevant, particularly as denoted by the difference between SST and the air temperature at 500 hPa (SST-T500) [see in this regard *Bracegirdle and Gray*, 2008], which can be considered an indicator of convective tropospheric heating driven by surface fluxes. The low-level baroclinicity is assessed through the horizontal temperature gradient at 850 hPa (T850). In the following sections, daily anomalies for the fields of temperature, geopotential height, and surface wind are computed from ERA-I as well as for the potential vorticity (PV) at 300 hPa, the latter considered to be an indicator of stratospheric intrusions [e.g. *Claud et al.*, 2004]. If environmental conditions favor deep penetration of an upper level PV anomaly, it can induce spin-up from a conditional neutral atmosphere [*Montgomery and Farrell*, 1992] or enhance existing surface vorticity [*Rasmusson and Turner*, 2003] and eventually cause PLs to form.

2.3. Arctic Sea Ice Concentration

[17] Sea ice concentrations generated from brightness temperature data derived from the Nimbus-7 SMMR and DMSP SSM/I radiances [*Cavalieri et al.*, 1996] are utilized. These data can be found at <http://nsidc.org/data/nsidc-0051.html> and are provided on a polar stereographic projection at a grid cell size of 25×25 km. We use this information to define the sea ice mask (represented here by the maximal monthly ice extension with a concentration greater than 85% over 1979–2007).

2.4. Methodology

2.4.1. Calculation of Anomalies Associated with PL Formation

[18] In a first step, mean fields of the above-described variables are calculated for cold season months (ONDJFM) over the period specific to each considered PL dataset, both

for all days of the period and for PL key days. The standardized anomaly field corresponds to the difference between these two fields, divided by the standard deviation calculated over the whole period. The statistical significance of the results is assessed using a phase-scrambling bootstrap test with 999 samples [*Davison and Hinkey*, 1997]. For the wind at 925 hPa, which is a vector field, the standardized anomaly is calculated for each component, as well as its significance. By convention, the vector significance corresponds to the most significant component.

[19] To show the evolution of the anomaly patterns, each anomaly field for each day during a 9 day window centered on the key day (i.e., key day -4 through key day +4) is calculated, using the same procedure as described above.

2.4.2. Weather Regimes

[20] Determination of WR is performed over the North Atlantic-Europe domain (NAE, 20°N – 80°N / 90°W – 30°E) by an objective analysis based on clustering techniques for Z500 NCEP-NCAR daily maps in the boreal winter (November–March) of 1957–2011. Cluster analysis is a multivariate statistical technique that aggregates a set of events into limited states according to similarity criteria; by construction, it accounts for time scale interactions and spatial asymmetries [*Anderberg*, 1973] of the circulation patterns. The partition algorithm in the NAE sector traditionally leads to four clusters [e.g., *Cassou*, 2008], the number of clusters being established according to statistical tests based on reproducibility issues [*Michelangeli et al.*, 1995], and sampling dependence and variance ratio consideration [*Straus et al.*, 2007]. Each day in the selected period is classified into one of the four regimes [*Cassou et al.*, 2011]. In addition, several classifications based on the minimum similarity distance between Z500 daily anomaly patterns and pre-existing centroids have been performed considering either Euclidian or correlation distances applied either in the phase space or in the physical space. The results presented here are not dependent on the retained atmospheric fields or on the distances. Consequently, in this paper, we use only regimes calculated on Z500 based on the Euclidian distance in the phase space. The distance to the closest centroid (intra-regime distance) gives information about the differences in the anomaly magnitude and spatial departure between a given day and its associated centroid. The distances to the other centroids (inter-regime distances) quantify the relative position of the anomalous daily circulation with respect to the other regimes. Over the North Atlantic-Europe domain, the WR approach is applicable only for winter and summer months [*Cassou et al.*, 2011]. For the intermediate seasons, the North Atlantic circulation cannot be classified according to statistical significance tests. Consistently, PLs that form in October and in April–May are excluded (22 cases out of 156 for Noer's list; cf. Table 1) from the following.

[21] Zonal (ZO) and Greenland-Anticyclone (GA) WRs are characterized by a strong negative (respectively positive) anomaly near Greenland and Iceland, and a positive (respectively negative) anomaly at lowest latitudes of the North Atlantic Basin (see Figure S1 in the supporting information, representing the four wintertime WR centroids). These two regimes represent the positive and negative phases of the North Atlantic Oscillation, and will be referred to accordingly in this paper. NAO+ (versus NAO-) is characterized by an intensification (versus weakening) of the Azores High and a

deepening (versus slackening) of the Icelandic Low [Cassou, 2008] and corresponds to the north/south modulation of the North Atlantic westerly mean flow. The SB regime (Figure S1, top right) is dominated by a strong positive anomaly over Scandinavia and Northern Europe, while low pressure prevails in the Labrador Sea; for AR, the anomalous high is observed South of Greenland (Figure S1, bottom right) encompassing a large part of the North Atlantic, while negative anomalies extend from Spitsbergen to the Mediterranean Sea.

[22] For all PL dates, the regime to which each belongs is determined and an accumulated distribution deduced.

3. Chronology of PL Formation

3.1. The Norwegian and Barents Seas

[23] Figure 2 displays the standardized composite anomalies determined from ERA-I of key variables for the *Noer et al.* [2011] PL formation dates over the Barents and Norwegian Seas. The large-scale environment corresponding to PL development there comprises a large and significant Z500 negative anomaly over the formation area (absolute anomaly maximum value of -126 m), a significant positive anomaly of SST-T500 over the Nordic Seas from the ice edge to Scandinavian and Icelandic coasts (absolute anomaly maximum value close to 5°C), and large T850 gradients indicating baroclinicity (approximately $0.5^{\circ}\text{C}/(100 \text{ km})$). The PV at 300 hPa presents a positive anomaly (absolute anomaly maximum value around 1.2 PVU ; $1 \text{ PVU} = 10^{-6} \text{ m}^2 \text{ s}^{-1} \text{ kg}^{-1} \text{ K}$), which is significant over a smaller area compared to Z500, mostly confined to the ocean. Furthermore, the Norwegian and Barents Seas are dominated by anomalous north-northeastly 925 hPa wind, with a significance larger than 90% and maximum velocity absolute anomaly of about 6 m s^{-1} . The

SST does not differ significantly from its climatological value (not shown). This is expected though because of its longer variation timescale compared to both atmospheric fields and PL dynamics and because of the relatively low accuracy and coarse spatial resolution of the SST analysis at these latitudes.

[24] The time evolution of the atmospheric anomalies is now presented for around the key day. The Z500 standardized anomaly (Figure 3) shows a weak, but statistically significant, structure north of the Barents Sea up to 4 days before the key day. This feature gradually intensifies and expands over the whole Barents Sea first and then over the Norwegian Sea spreading towards Iceland, until the key day and key day +1. Then the negative anomaly decreases, the maximum amplitude progressively slides to the south, the westward extension reduces, and finally, the anomaly disappears by key day +4. It should be noted that positive anomalies are concomitant from the Irminger Sea to Western Europe; these tend to extend northwestward with PL development. The negative anomaly reaches its maximal amplitude on key day +1, with an absolute anomaly value of -135 m. This temporal behavior has already been noticed by Businger [1987], who found slightly larger anomaly values (-140 m) for the key day and -165 m on the day after. A similar behavior prevails for SST-T500 over the open sea part of the Barents and Norwegian Seas (not shown). The near-surface wind chronology (Figure 4) shows a significant north-northwesterly anomaly over the Norwegian Sea and the western part of the Barents Sea up to key day -3. This anomaly increases in intensity until a day after the key day, reaching a maximum absolute anomaly value of 7.5 m s^{-1} , with a gradual rotation of the direction feature: the westerly component vanishes (except over the southern Norwegian Sea) and is gradually replaced by an easterly component that is

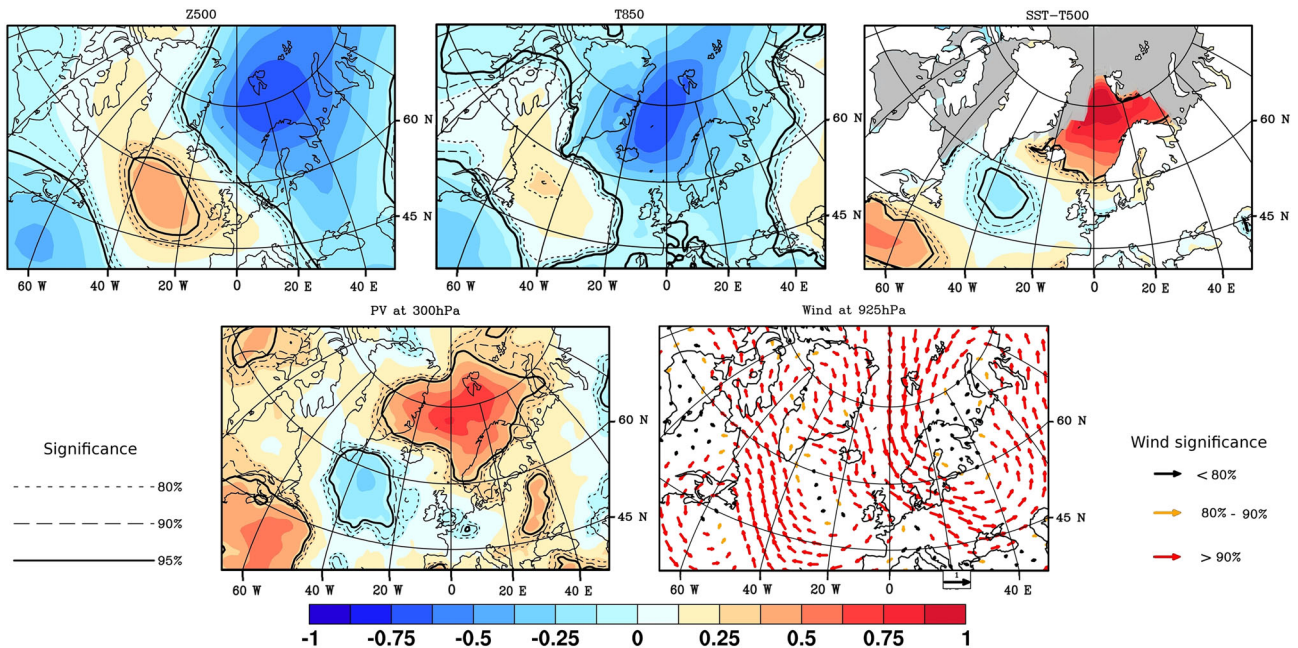


Figure 2. Composite standardized anomalies of Z500, T850, SST-T500, PV at 300 hPa, and wind at 925 hPa in cold season months (ONDJFM) for PLs key days from Noer's (date) list. Gray areas correspond to maximal monthly sea ice extent from 1979 to 2007. The significance levels are indicated by solid and dotted lines (scalar fields) and the color of the arrows (wind).

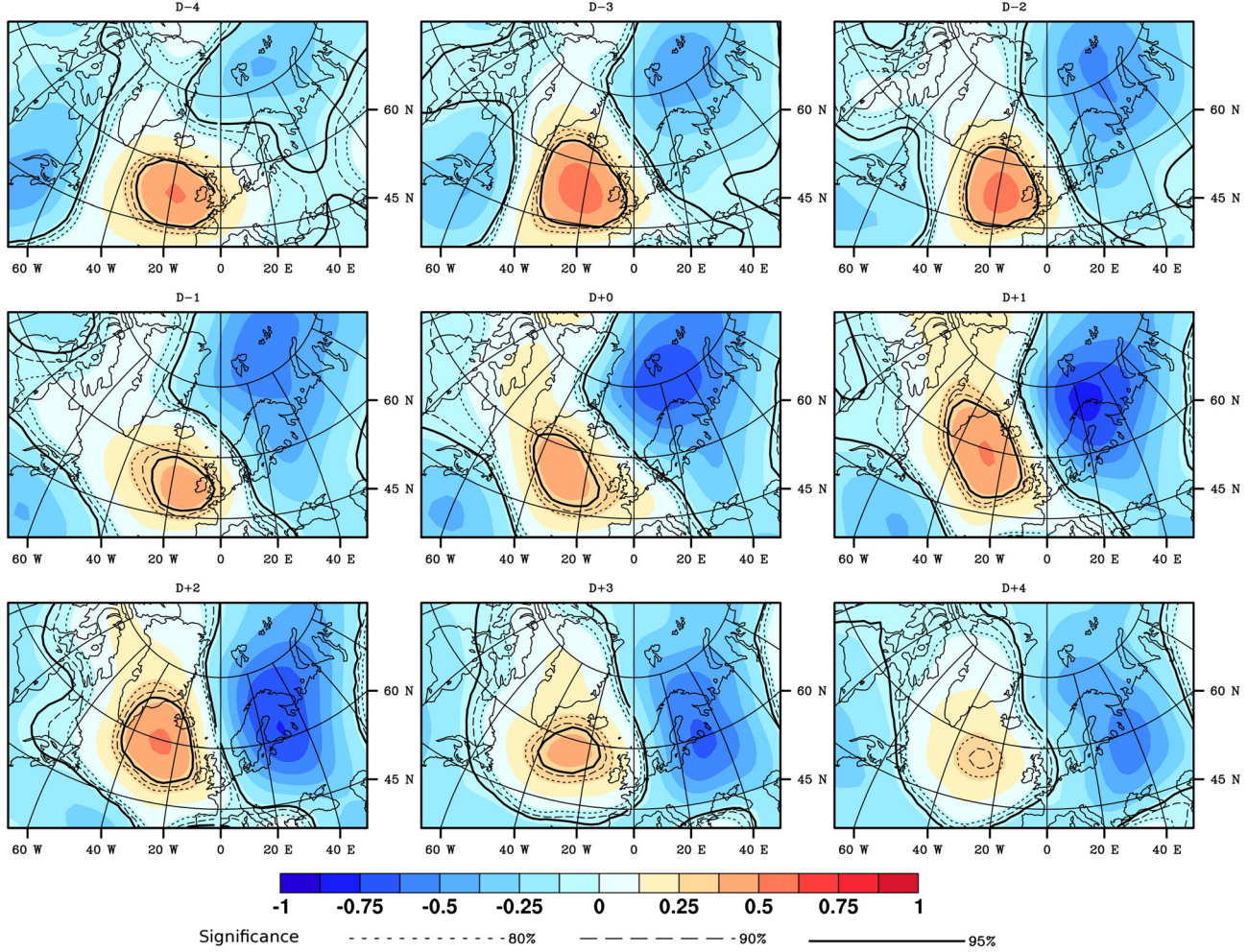


Figure 3. Evolution of the Z500 anomaly field from 4 days before key day to 4 days after, according to Noer's (date) list, for cold season months (ONDJFM), from 2000 to 2011.

particularly strong over the Barents Sea penetrating into Europe. Then the overall amplitude decreases, becoming very weak by key day +4. For PV at 300 hPa, the anomaly already exists by 4 days before the PL formation day, but it increases just before the key day (not shown). On key day +2, the anomaly diminishes and vanishes. Signs of baroclinicity, as enhanced horizontal gradients of T850, mainly appear on the key day (not shown). To summarize, a tropospheric environment favorable to PL formation exists for an approximate 8 day window centered on the PL life span. The PL outbreak day (i.e., the key day) corresponds to a sudden intensification of anomalies, particularly in terms of near-surface wind and PV.

[25] We conduct separately similar composite analyses for PLs that formed over the Norwegian Sea (87 cases) and those that formed over the Barents Sea (47 cases). Although some anomaly features differ in detail (Figure 5), Z500 and SST-T500 anomalies are always centered over the PL formation region. Anomalies have larger amplitude in the case of Barents Sea PLs, which might be related to the smaller size of the sample. Concerning near-surface winds for the Barents Sea cases, the anomaly mainly presents an easterly component on the eastern side of the PL formation zone, indicating that a majority of PLs in the Barents Sea is formed in cold air

outbreaks from the areas between Spitsbergen and Novaya Zemlya. For the Norwegian Sea cases, the wind anomaly is northerly, reflecting the fact that PLs mainly form in cold air outbreaks from the Fram Strait. Low-level baroclinicity is observed over a longer time period (from key day -3 to key day +1) for the Barents Sea PLs than those for the Norwegian Sea (key day and key day +1). This is consistent with the stronger baroclinicity of Barents Sea PLs compared to Norwegian Sea PLs found by *Bracegirdle and Gray [2008]*.

[26] Figure 6 displays the evolution in the vertical of 600 hPa to 200 hPa PV anomaly cross sections for a latitude of 71.25°N (the median latitude of PL cases in Noer's list) and longitudes ranging from 80°W to 40°E (for the Norwegian Sea cases) and from 45°W to 80°E (for the Barents Sea cases). For the Norwegian Sea cases, the first significant pattern appears the day before the key day, between 500 hPa and 300 hPa over the Norwegian Sea around 10°E, and rapidly grows into a larger structure with a vertical extension from 550 hPa to 200 hPa and horizontal reach from 30°W to 20°E, for the key day until 2 days after. Once again, the maximal extension and intensity of the anomaly are found for key day +1. This is not the case for the Barents Sea PLs, for which strong and significant precursors already exist around 400 hPa from up to 4 days before the key day over

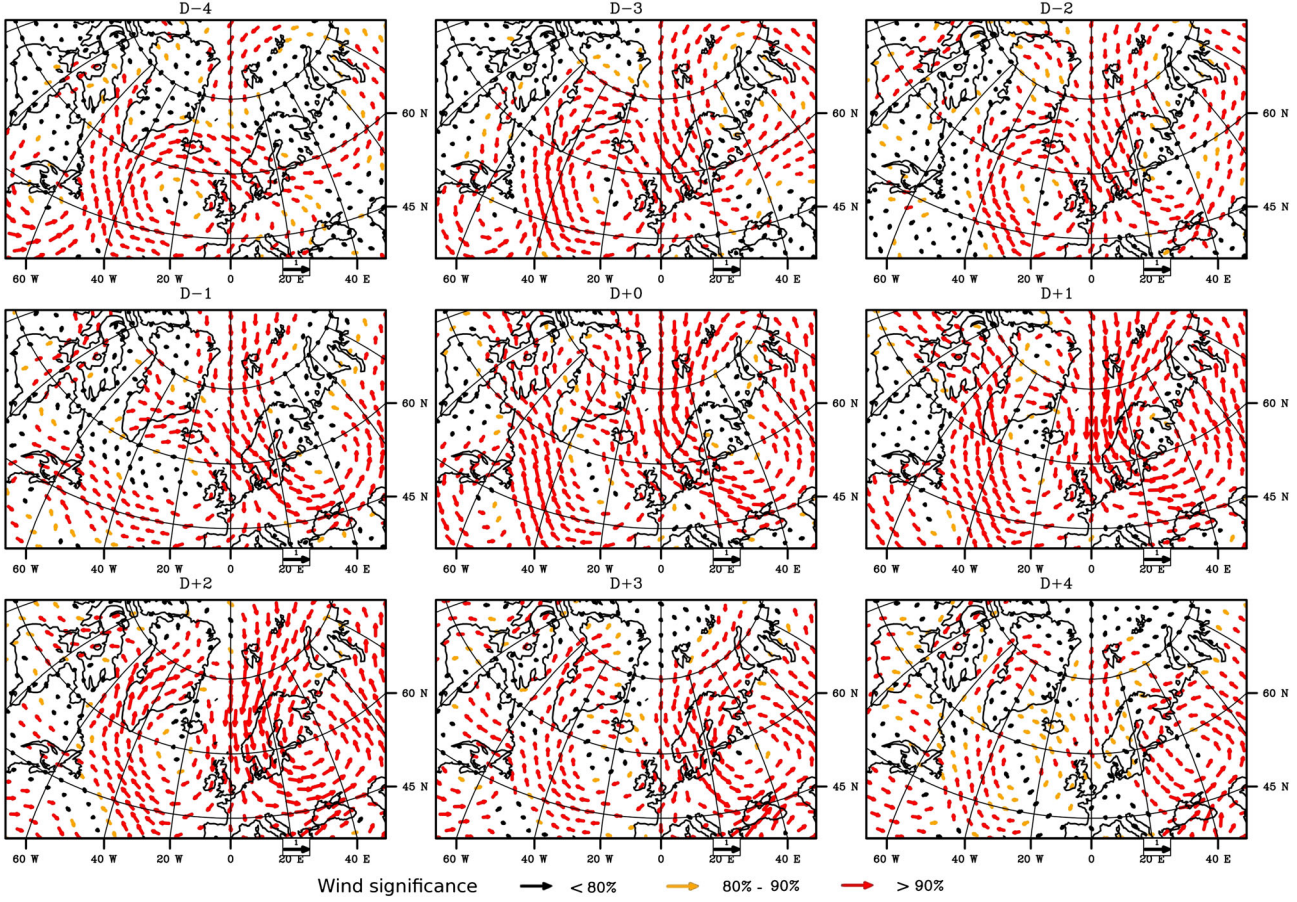


Figure 4. Similar to Figure 3, but for the wind at 925 hPa.

the Greenland Sea, and which gradually shift to the east until the key day, when the significant anomaly covers the Norwegian and Barents Seas. This anomaly rapidly decreases by key day +2 (not shown).

[27] Similar analyses conducted on the other PL databases covering this area confirm the above results (not shown), although with local differences: the anomalies are generally weaker before the key day, particularly for Wilhelmsen's cases, and have a longer persistence, staying strong and significant for up to 3 to 4 days after the key day. This difference may be due to the lower accuracy on determining the outbreak dates than for the most recent lists and/or to a less reliable reanalysis (before 1979, satellite data were not assimilated). Moreover, for Wilhelmsen's and Businger's PL cases, the Z500 anomaly formed further south-east than in the present analysis. This may be related to the geographical location of the PLs in each dataset (Table 1).

3.2. The Labrador Sea

[28] The observational study by Rasmussen *et al.* [1996] showed that PLs forming over the Labrador Sea are remarkable because of their similarity in terms of common satellite-observed cloud signature, associated synoptic conditions, and physical mechanisms. Figure 7 displays the standardized anomalies of key variables for key days from Kolstad's list and confirms this intuition. The characteristic environment for PL formation in this region is marked by

strong and significant anomalies centered over the eastern Labrador Sea, along the Greenland coast, and covering the entire Labrador Sea, Greenland, and the Greenland Sea between 55°N and 80°N. Similar to the Noer's cases in the Norwegian and Barents Sea, the anomalies are negative for Z500 and T850 but positive for SST-T500 and PV at 300 hPa. The wind anomaly is strong and from the northwest over Hudson's Bay and Nunavut, and mostly westerly over the Labrador and southern Irminger Seas. The particularly strong wind anomaly over the Hudson Strait confirms the wind channeling effect of the topography, as described by Rasmussen *et al.* [1996]. Note also that the Greenland elevated terrain influences the low-level flow [e.g., Doyle and Shapiro, 1999].

[29] A strong Z500 negative anomaly appears 6 days before the key day over a large area including Hudson's Bay, Hudson Strait, North Quebec, and the northwestern part of the Labrador Sea (Figure S2 in the supporting information). This anomaly propagates over northern Greenland by key day -3, and extends up to the Greenland Sea on key day -2. From 3 days before the key day onwards, the wind anomaly over the Hudson Strait gradually becomes established. Just before the key day, the Z500 anomaly settles over the Labrador Sea, and a SST-T500 anomaly appears near the ice edge (Figure S3 in the supporting information). Thus, PL outbreaks in this region correspond to the onset of the SST-T500 significant anomaly and the sudden intensification of PV at 300 hPa,

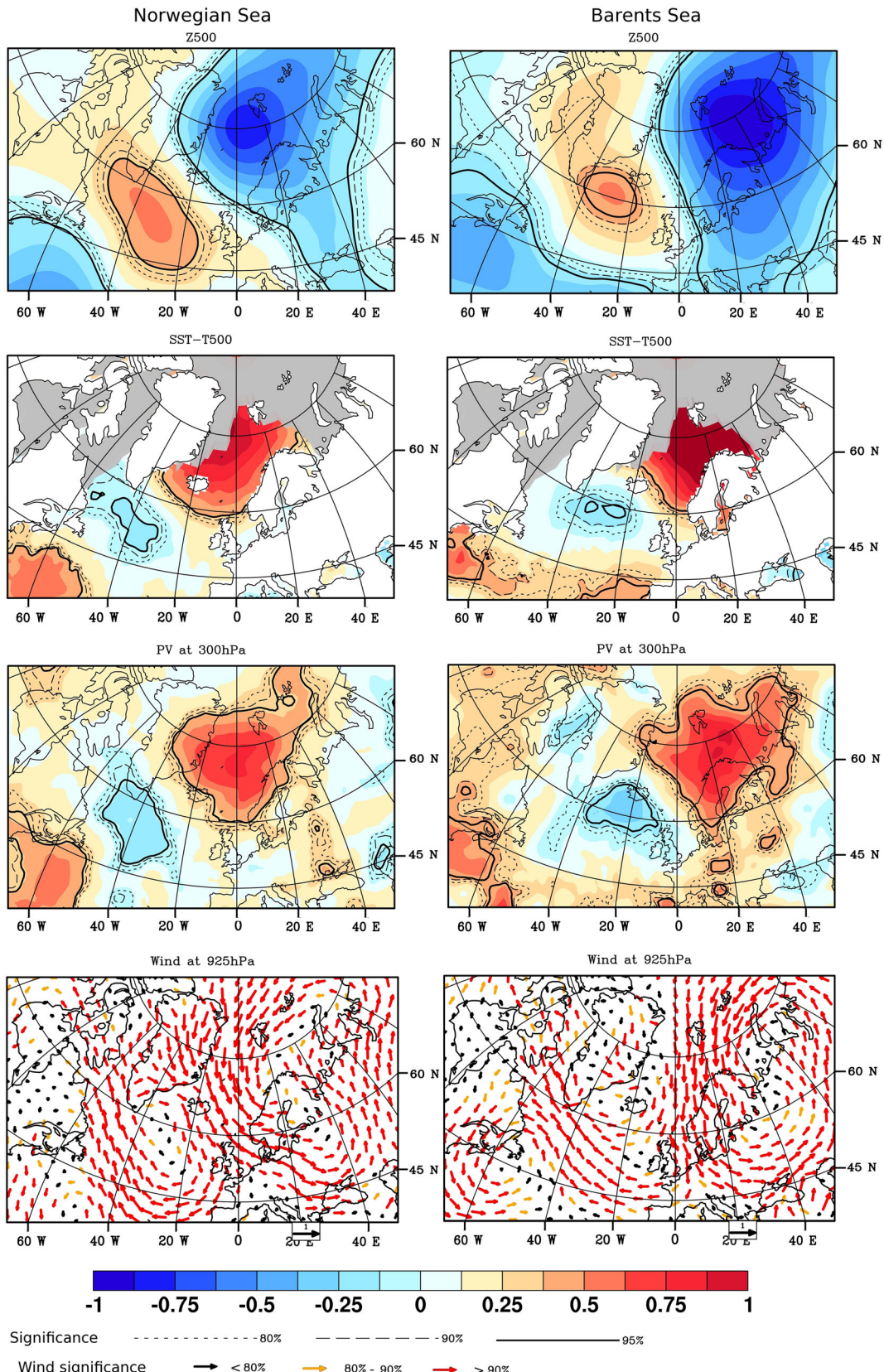


Figure 5. Comparison between composite standardized anomalies of Z500, SST-T500, PV at 300 hPa, and wind at 925 hPa in cold season months (ONDJFM) for key days, according to the formation location: the Norwegian Sea on the left side and the Barents Sea on the right side. The significant levels are indicated by solid and dotted lines (scalar fields) and the color of the arrows (wind).

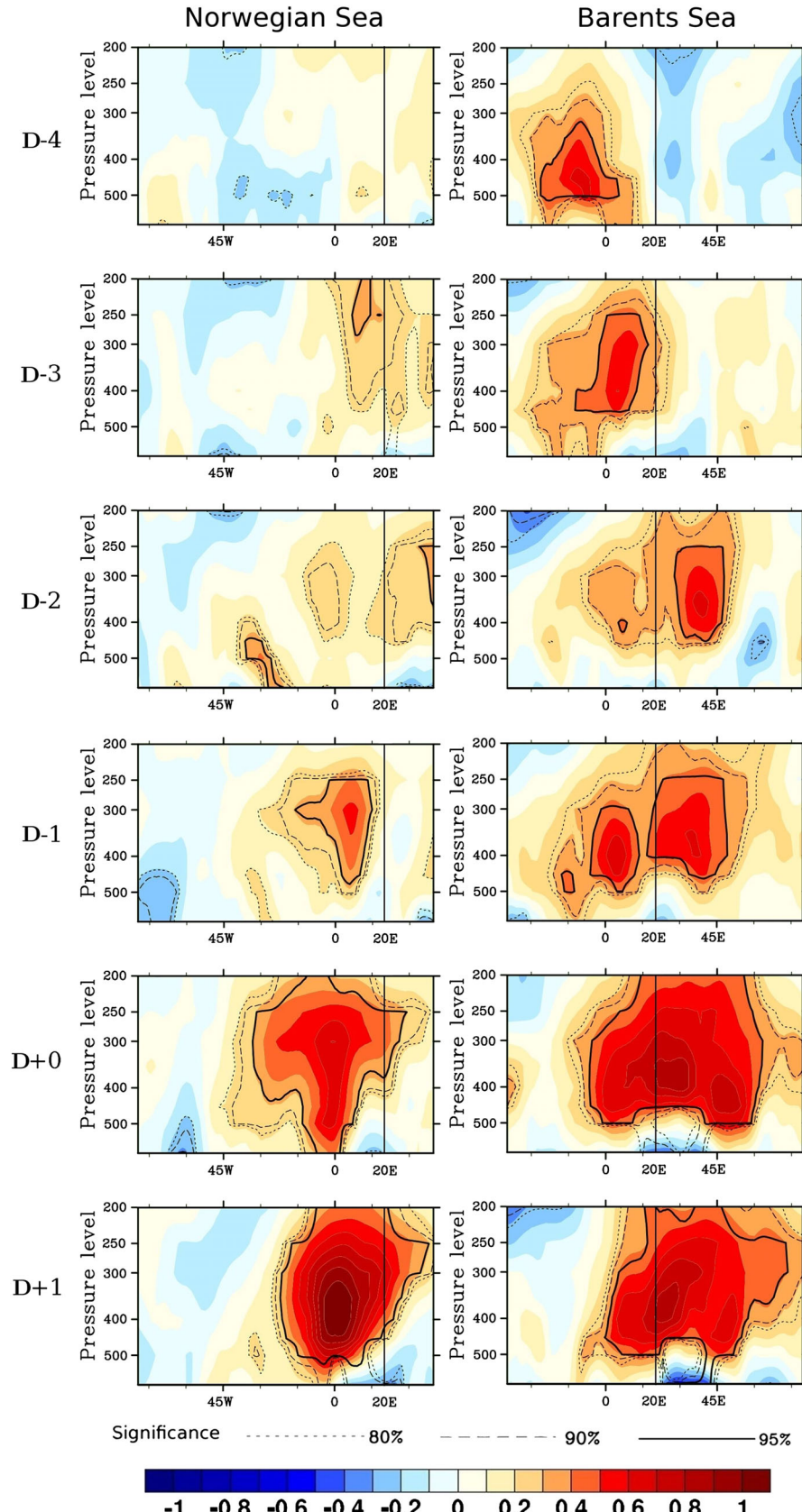


Figure 6. Comparison between the evolution of vertical (600–200 hPa) PV composite standardized anomalies from 4 days before key day to 1 day after according to formation location: the Norwegian Sea on the left side and the Barents Sea on the right side. The west-east cross section was taken at 71.25°N. The vertical line at 20°E corresponds to the approximate delimitation between the two seas. The significant levels are indicated by solid and dotted lines.

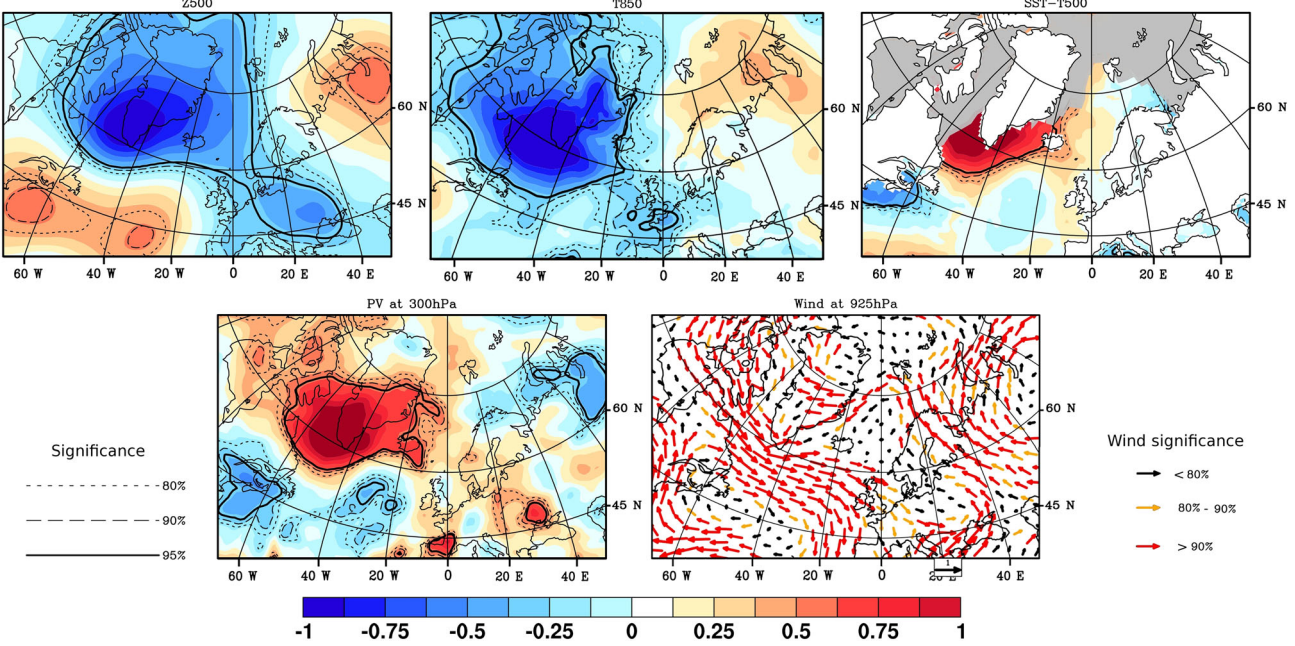


Figure 7. Similar to Figure 2, but for Kolstad's list.

which previously existed over the Hudson Bay and Hudson Strait 6 days before, but was very weak (not shown). After the key day, the anomalies extend over the Atlantic Basin between 55°N and 80°N , and between the Canadian coast eastward to the Greenwich meridian. Persisting over the same area, the anomalies gradually decline.

4. WR and PLs

4.1. Links Between PL Occurrences and WR

[30] For each PL of the considered PL inventories, we determined its associated regime. The distributions by WR are shown in Figure 8, in blue for the Norwegian and Barents Seas and in orange for the Labrador Sea. About two third of Noer's PL cases formed in the AR and NAO- regimes (37% with 49 PLs in AR and 28% with 37 PLs in NAO-), while 19% formed in NAO+ (26 PLs) and 16% in SB (22 PLs). This unequal distribution of PLs by WRs cannot be simply explained by the mean occurrence of the four regimes over the specific 1999–2011. Indeed, those are equal to 30% (571 days) for NAO+, 23% (443 days) for SB, 21% (404 days) for NAO-, and 26% (487 days) for AR, as represented by the dots in Figure 8. That is, a PL formation was observed over this period for nearly 10% of days in NAO- and in AR, whereas they were half as frequent for NAO+ and SB. Thus, the NAO- and AR regimes can be interpreted as large-scale anomalous circulations favorable to PL outbreaks, while NAO+ and SB tend to be PL-averse. A similar behavior is found when considering the Norwegian and Barents Sea PLs separately, with more PLs forming in SB over the Barents Sea (21%) than over the Norwegian Sea (14%).

[31] Consistent results are obtained for the other datasets (Figure 8, in blue) despite the different time periods and slightly different geographical domains: AR is always the most and SB the least represented WR, with

NAO- and NAO+ being approximately equivalent in terms of PL occurrence.

[32] For the Labrador Sea (Figure 8, in orange), the vast majority of PLs formed in NAO+, with 74% of cases for the Kolstad list, while they were only 16% as frequent during SB and 11% for AR days, with none in NAO-. The Parker list for the same region gives a consistent distribution for another period, confirming the robustness of this result.

4.2. WRs as Conditional Large-Scale Dynamics for Norwegian and Barents Seas PL Formation

[33] To understand the physical reasons for the statistical link between PLs and WR occurrence, the conditions associated with each WR must be investigated. In particular, the mean states of Z500, SST-T500, and wind at 925 hPa specific to each WR provide information that is important for PL formation and intensification as discussed above. For AR, the Norwegian and Barents Seas are characterized by a negative anomaly of Z500 (Figure S1, in the supporting information), a positive anomaly of SST-T500 corresponding to reduced low-level atmospheric stability (Figure S4), and an easterly wind anomaly with a northerly component over the Norwegian Sea (Figure S5). These large-scale atmospheric conditions are representative of the tropospheric conditions favorable for PL formation over the Nordic seas, where a key process is the advection of cold arctic air across gradually warmer sea surface. Consequently, this supports the noticeably larger occurrence of PLs observed for AR days, as well as of the more western PL formation area than those of the other regimes (not shown).

[34] Anomaly patterns for the NAO- mode are similar for the typical PL formation environments of both the Norwegian Sea and Barents Sea. The SB environment bears no resemblance to the typical PL trigger factors; it is associated with southerly flow along the Norwegian coast and from

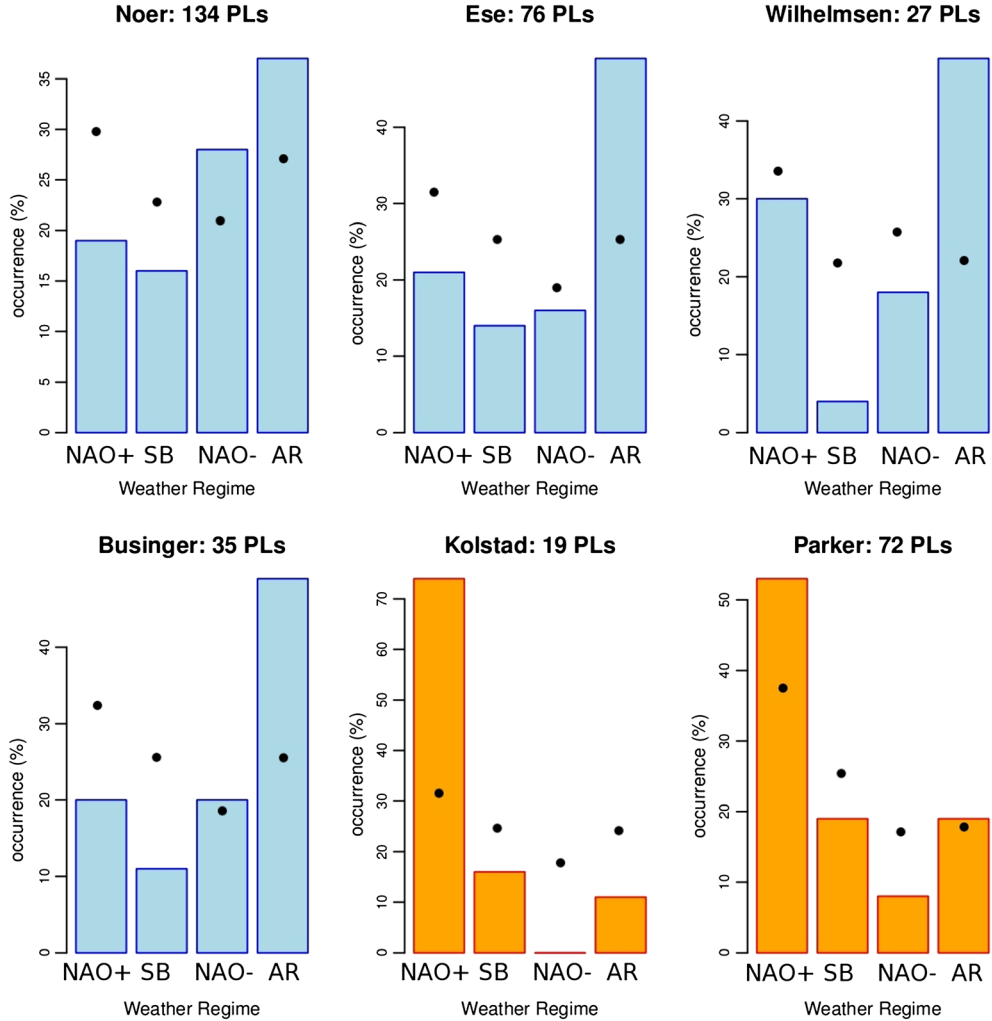


Figure 8. PL occurrence distribution according to WR corresponding to key days, for the Norwegian and Barents seas (in blue) and the Labrador Sea or adjacent to the southern coast of Greenland (in orange): Noer’s cases (1999–2011), Ese’s cases (1971–1983), Wilhelmsen’s cases (1978–1982), Businger’s cases (1971–1983), Kolstad’s cases (2000–2009), and Parker’s cases (1977–1994). WR occurrences during corresponding periods are indicated by the black dots.

northern Scandinavia and Kola mainland, and advection of air masses toward colder sea surface. For NAO+ the situation is spatially contrasted: the decreased low-level stability and the northerly winds tend to favor PL formation on the western side, while they clearly inhibit PL formation in the Barents Sea.

[35] We further tested the possibility that PLs are associated with specific WR transitions, as postulated for local extreme precipitation events in the Mediterranean basin [Sanchez-Gomez *et al.*, 2008]. The chronological mean distribution of regime occurrences is plotted for PLs in each regime, from 6 days before the PL outbreaks to 4 days after (Figure S6). Over this temporal window, minor departures from symmetry with respect to the key day are evident, but their statistical significance is difficult to assess, considering the number of PLs and the shortness of the period. For the NAO+ mode PLs, the days following outbreaks (i.e., from key day +1) are less likely to be NAO+ than the preceding days, suggesting that PL formation occurs preferentially in the decaying phase

of the regime. The opposite is found for AR; that is, PLs form in the earlier stages of the regime. SB is least comparable to the other regimes because the proportion of days in the same regime drops rapidly both before and after the key day. To further examine this feature, the same analyses were performed considering regimes with at least 5 days persistence and excluding the first and last days of the regime event, in order to eliminate transient and ambiguous episodes [as in Michelangeli *et al.*, 1995]. In that situation, the results are only changed for SB in which the PL occurrence drops from 16% to 12%. This tends to confirm that SB large-scale conditions are globally PL-averse and that PL cases could fall into the SB pool by chance because all days are classified by construction.

[36] Another way to illustrate this point is to examine the intra- and inter-distances to the regimes, for key days of PL belonging to each regime and to compare them to the climatological distribution (Figure 9). This metric objectively quantifies the degree of similarity between large-scale PL key days and WR average dynamics. Our results show that

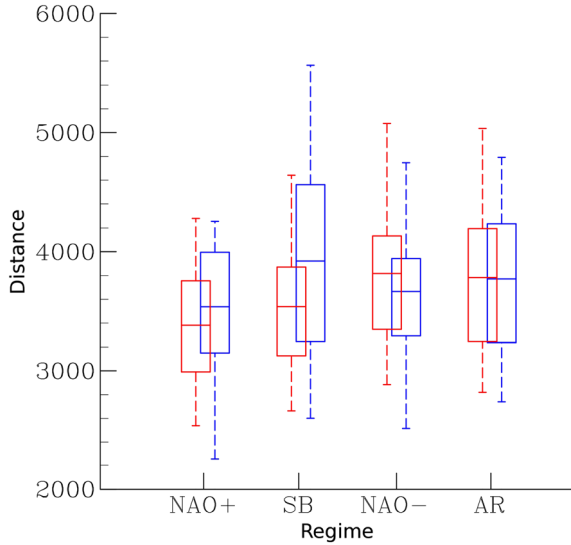


Figure 9. Comparison between intra-regime distance distributions for key days (in blue) from Noer’s list and intra-regime climatological distributions (in red). The horizontal line within the box corresponds to the mean; bottom and top box bounds show the 25th and 75th percentiles, respectively; bottom and top whisker bounds indicate the 5th and 95th percentiles, respectively.

the intra-regime distances for PLs in SB are highly different from their mean distribution, indicating a strong departure either in intensity or spatial location, or both, of the related

Z500 anomalies versus the mean SB centroid. Increased distances are also found for NAO+ PL days but to a lesser extent. By contrast, for AR, the two distributions of distances are not differentiable statistically while NAO- results suggest that PL days occur for conditions rather close to the centroid. The SB inter-regime distance distributions when PLs occur in other regimes always present larger values than their climatological distributions (not shown), suggesting again that PLs form when conditions are notably different from SB mean conditions.

[37] Because the Euclidian distance is an integrated quantity that accounts for the field anomaly over the whole considered area, it may mask important local information. Figure 10 shows the difference between Z500 anomaly patterns for PL formation days as a function of regime occurrence and the corresponding centroid of that regime. These maps correspond to the spatial signatures of the distances previously detailed. The NAO- does not display marked patterns, in agreement with the reduced intra-regime distances in Figure 9. By contrast, NAO+, SB, and AR present strong negative patterns centered over the PL formation area of the Norwegian and Barents seas. For AR (Figure 10, bottom right), the departure pattern corresponds to an enhancement of the mean negative core over Scandinavia. For NAO+ (Figure 10, top left), it indicates a bulge to the east of the NAO+ characteristic Icelandic low-pressure anomaly, but the outer anomalies are of opposite sign with respect to the mean centroid. For SB (Figure 10, top right), the departure pattern is very pronounced and is opposite in sign to the typical anticyclonic SB pattern over the Norwegian and Barents Seas. The spatial correlation

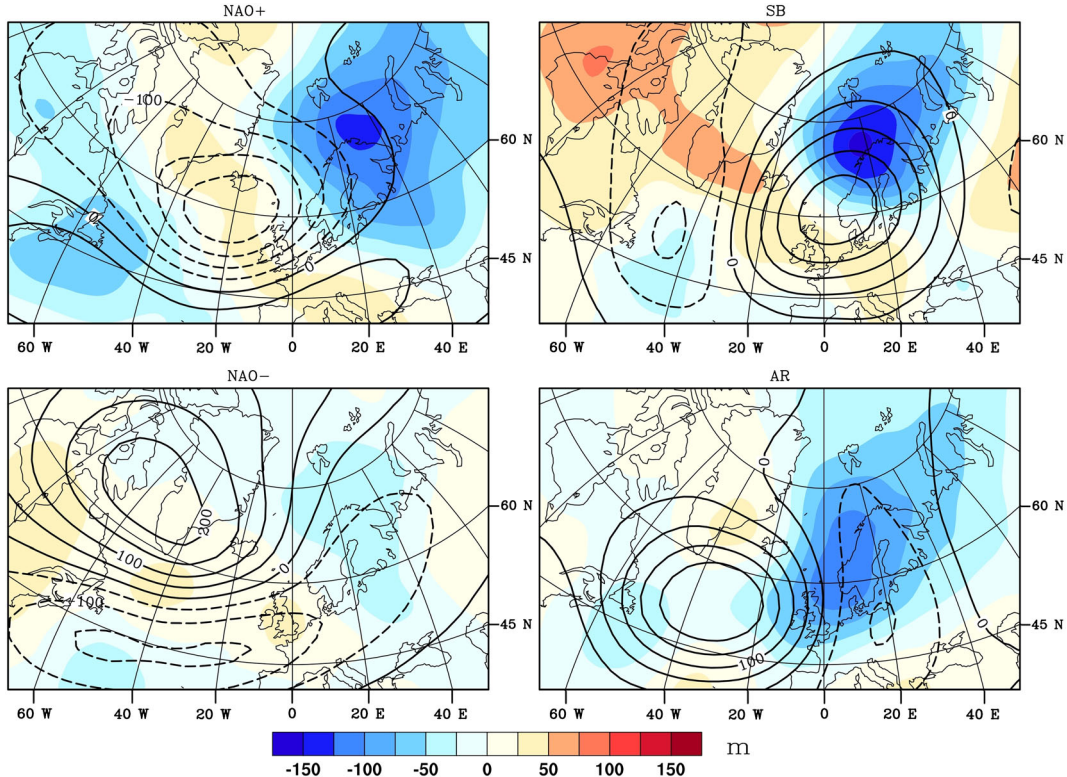


Figure 10. Difference between Z500 anomalies patterns for the PL key day corresponding to each regime and the corresponding regime Z500 anomaly pattern. The latter is represented by black contours (dotted contours for negative values).

between the centroid and the composite built on PL occurrence for SB is consistently equal to -0.40 . Thus, PLs forming in SB do so during a “weak” regime of that type. The large-scale dynamics are then characterized by a much weaker Scandinavian blocking high consistent with a lower amplitude trough over Greenland and the Labrador Sea.

4.3. Specifics of Large-Scale Environment of PLs According to WRs

[38] In this subsection, we show the composite atmospheric conditions prevailing on PL days in the Norwegian and Barents Sea (Noer’s dataset), separately for each regime. The standardized anomalies of Z500, SST-T500, wind at 925 hPa, and PV at 300 hPa are displayed for PL formation days classified as AR (Figure 11), NAO– (Figure 12), NAO+ (Figure 13), and SB (Figure 14). We note different large-scale patterns, corroborating the concept of a continuum of conditions leading to PL formation.

[39] For AR cases (Figure 11), the PV anomaly is noticeably stronger over the Norwegian Sea than for the other regimes, and the wind anomaly is southward. Composites of SST-T500 and T850 indicate enhancement of the convective tropospheric heating by surface fluxes and of baroclinicity over both the Norwegian and Barents seas.

[40] For NAO– cases (Figure 12), the Z500 anomaly pattern is centered over Scandinavia, and the low-level wind has a northeasterly anomaly. A positive SST-T500 anomaly is particularly pronounced over the Barents Sea, and the T850 pattern indicates low baroclinicity, especially over the Norwegian Sea. Moreover, the PV anomaly is very weak south of Svalbard. These conditions suggest a great role of convection and a weak role of baroclinic interaction for PL developments in NAO–.

[41] Specificities of the environment for NAO+ cases (Figure 13) are a strong PV anomaly, signs of strong baroclinicity over the Norwegian Sea, the maximum of SST-T500 in the anomaly pattern that is confined to the west, and the northeasterly flow along the ice edge, together with an intensified low pressure to the south.

[42] PLs forming on days classified as SB show the most different environment from the general cases (Figure 14). The Z500 anomaly is weakly negative over the northern Norwegian and Barents seas and is positive south of the Norwegian Sea. There is almost no SST-T500 significant anomaly over the formation area, and the low-level wind displays a westerly anomaly south of 75°N but a northerly one to the north. The PV anomaly is confined to the western part of the area of interest. Despite the indications of baroclinicity, the full suite of conditions is consistent with the low proportion of PLs forming during this WR.

[43] Finally, Figure 15 compares the evolution of PV standardized anomalies from 4 days before the key day to 1 day following, according to the associated regime. For NAO regimes, PV anomalies are weakly positive and hardly statistically significant prior to the key day, as opposed to the negative centers that are strong and significant around 45°W . Moreover, the PV anomaly pattern associated with NAO– remains to the east of the PL formation position. Given that positive interactions between upper and lower tropospheric levels can occur only when a PV anomaly is located upstream [Hoskins *et al.*, 1985; van Delden *et al.*, 2003], PV may play little role in PL outbreaks. Using 6 hourly reanalysis data instead of daily data (not shown) results in a significant yet weak anomaly above the PL position 24 h before the key day for NAO+ and 6 h before for NAO–.

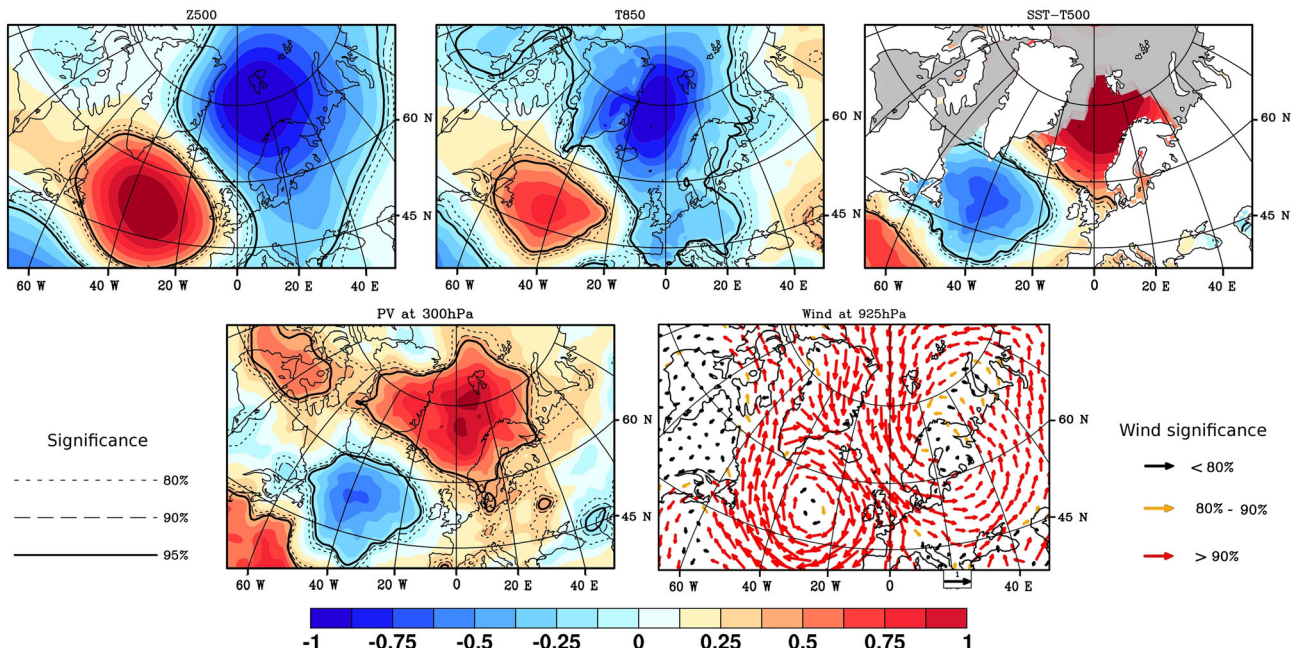


Figure 11. Composite standardized anomalies of Z500, T850, SST-T500, PV at 300 hPa, and wind at 925 hPa in cold season months (ONDJFM) for key days classified as AR (Noer’s list). Gray areas correspond to the maximum monthly sea ice extent from 1979 to 2007. The significance levels are indicated by solid and dotted lines (scalar fields) and the color of the arrows (wind).

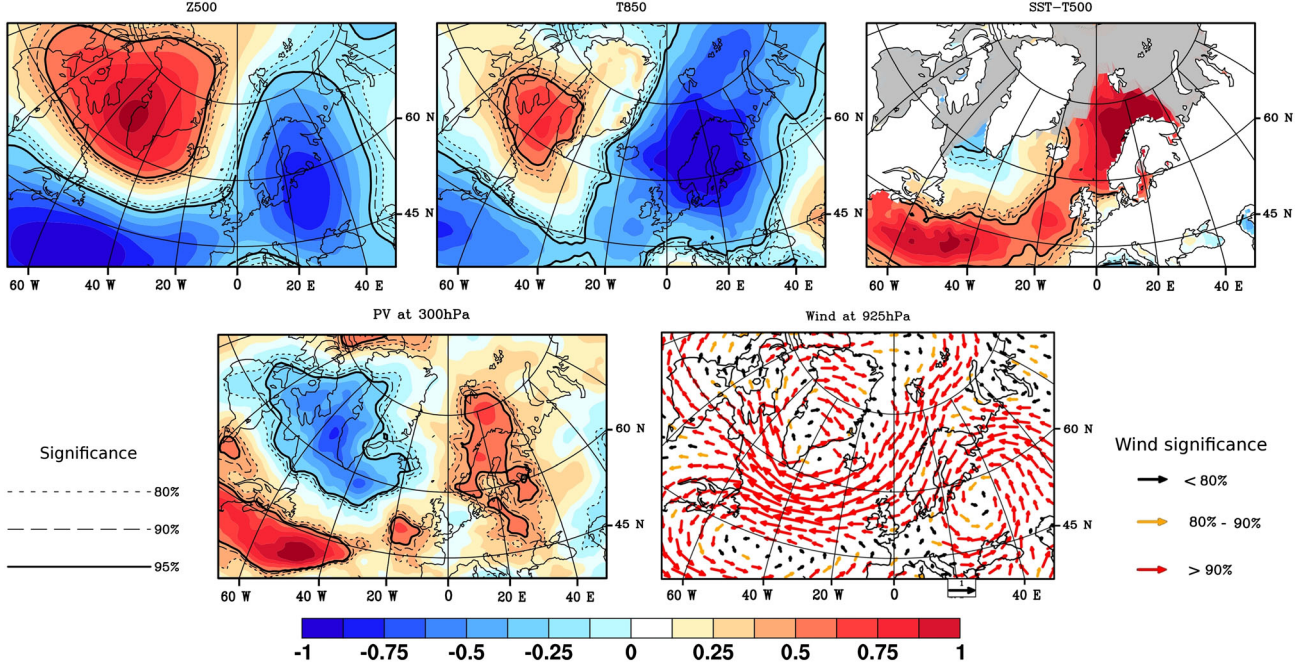


Figure 12. Similar to Figure 11, but for NAO-.

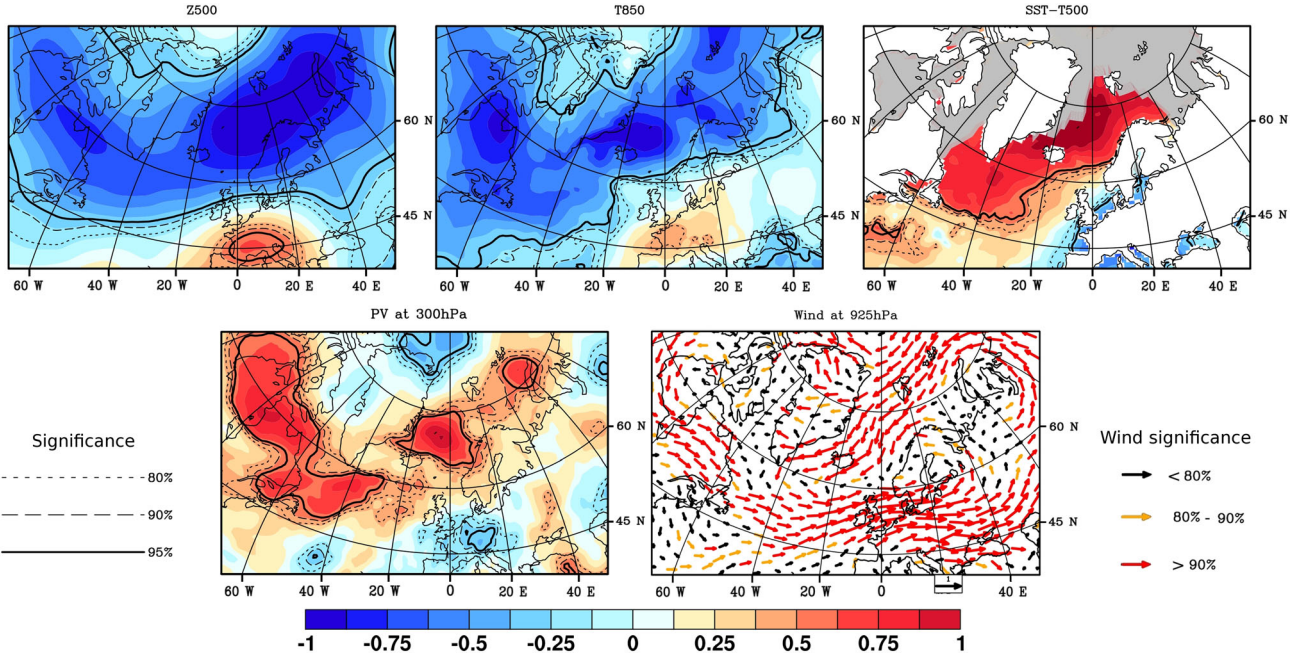


Figure 13. Similar to Figure 11, but for NAO+.

[44] For the SB and AR regimes, strong anomaly patterns exist from 2 days before the PL formation, and this is confirmed by the 6 hourly study. The anomaly forms above the formation area in the AR cases with a slight westward propagation, while for SB, it moves from the west, reaching the formation area only a few hours prior to PL formation. This feature suggests that PV is the main trigger for PL outbreaks during SB, consistent with the absence of a significant positive anomaly in SST-T500 (Figure 14) and the presence of unfavorable low-level wind anomalies.

5. Summary

[45] In this study, we determine the typical large-scale atmospheric circulation patterns conducive to PL development over the Norwegian/Barents and the Labrador Seas. Long-duration homogeneous datasets and state-of-the-art reanalysis products (ERA-Interim and NCEP/NCAR for the period before 1979) are utilized, allowing for statistical assessment of the results' significance. Variables examined in this study are the geopotential height at 500 hPa, the temperature at

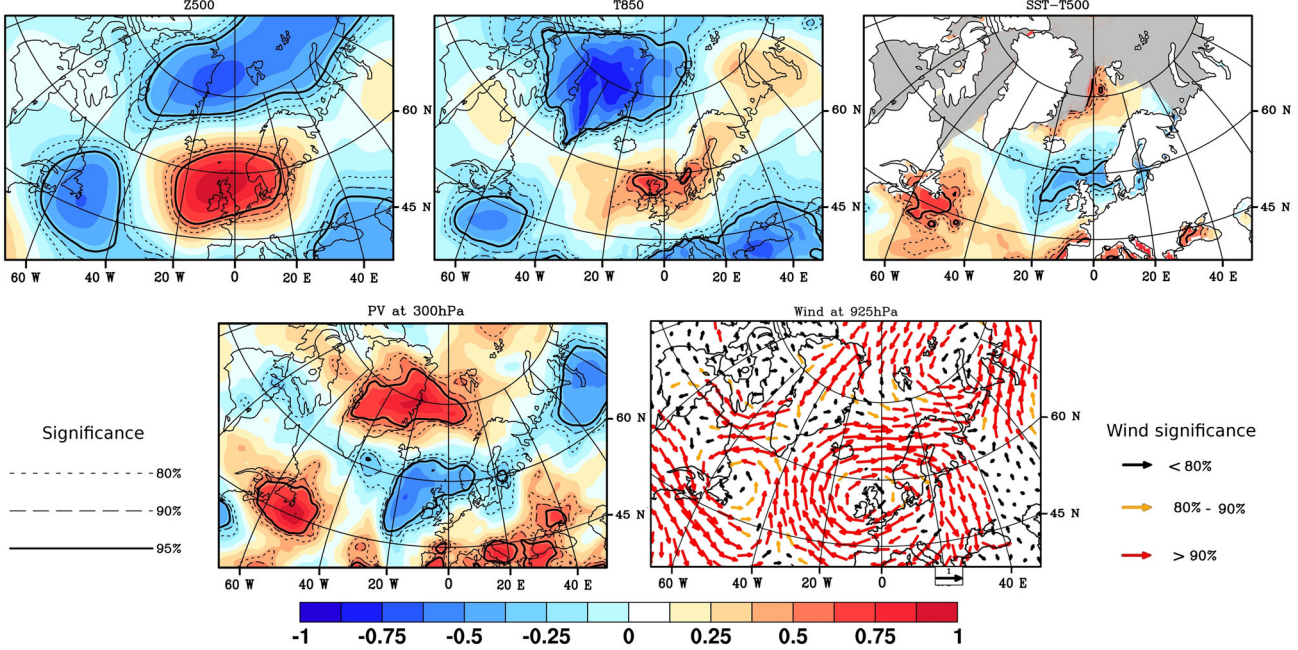


Figure 14. Similar to Figure 11, but for SB.

850 hPa, the wind at 925 hPa, the difference between the SST and air temperature at 500 hPa, and the potential vorticity at 300 hPa, all of which are known to influence polar low developments and are better represented in reanalyses than are the polar lows themselves [Condron *et al.*, 2006].

[46] We find that independent of the location of formation, broadly similar large-scale atmospheric patterns characterize the PL favorable environment: a negative anomaly of geopotential at 500 hPa, a positive anomaly of the difference between SST and the temperature at 500 hPa, and a positive PV anomaly at 300 hPa. The near-surface wind anomaly presents a different behavior according to the considered area, having a northerly main component over the Norwegian Sea, an easterly one over the Barents Sea, and a westerly one over the Labrador Sea when PLs occur. Low-level baroclinity is observed over a longer period over the Labrador and Barents seas (typically from 3 days before the key day to 1 day after) than over the Norwegian Sea (key day and the day after). The tropospheric environment becomes increasingly favorable for PL formation from 1 to 4 days before the outbreak and decreases between 2 and 4 days after, leading to the result that PLs occur when favorable conditions co-occur within an approximately 8-to-10 day window. We also show that PLs develop after a certain build-up, the outbreak day being marked by strong winds and PV intensification. For Norwegian Sea events, the PV anomaly—which indicates the presence of deep stratospheric intrusions—appears locally just before the outbreak, when lower atmospheric conditions are already favorable to PL outbreaks. This observation suggests that the upper anomalies trigger the maturation of PLs, probably by baroclinic interaction with the strong lower anomalies. For Barents Sea events, a deep PV anomaly several days before the key day forms near the Greenland east coast and moves eastward, reaching the Barents Sea 2 days before the outbreak, while other conditions may be PL-averse at this time. In this situation, PV anomalies likely contribute to

development of tropospheric PL-favorable conditions through destabilizing low-level layers and enhancing convective organization. For the Labrador Sea PL cases, both geopotential and PV anomalies form over the Hudson Bay around 4 days before the outbreak and reach the formation area on the key day. This one is marked by an intensification of positive SST-T500 and PV anomalies. All the anomalies reported above are significant at the 90% level (often higher), leading to the conclusion that well-defined large-scale environments promote PL formation; as such, the time evolution of the large-scale environment should help improve PL forecasting over these areas.

[47] Because winter WR over the North Atlantic and Europe have a 8–10 days persistence, similar to large-scale anomalies associated with PLs, their relationships to PL formation are also investigated. We find that PLs preferentially occur for some specific WRs. Over the Norwegian and the Barents seas, a PL formation is observed during winter months (1999 to 2011) on 10% of days in NAO– and AR, whereas their probability of occurrence is reduced by half that in NAO+ and SB. Consistent results are obtained for other PL datasets covering the same area for different periods, increasing confidence in our findings. In the Labrador Sea, according to two datasets covering different periods, more than half of PLs occur during NAO+ and almost none during NAO–. We further show that the synoptic environments on days classified into favorable versus unfavorable WR indeed correspond to conditions of key variables known to be particularly favorable versus less favorable for PL development over this area. We further document that no specific transitions between WR are related to a larger occurrence of PLs. Finally, we show that when PLs occur during an averse regime like SB, the anomalous large-scale circulation does not project very much onto the WR mean centroids or corresponds to a “weak regime” (e.g., for the SB regime, a weak and southward shifted blocking high).

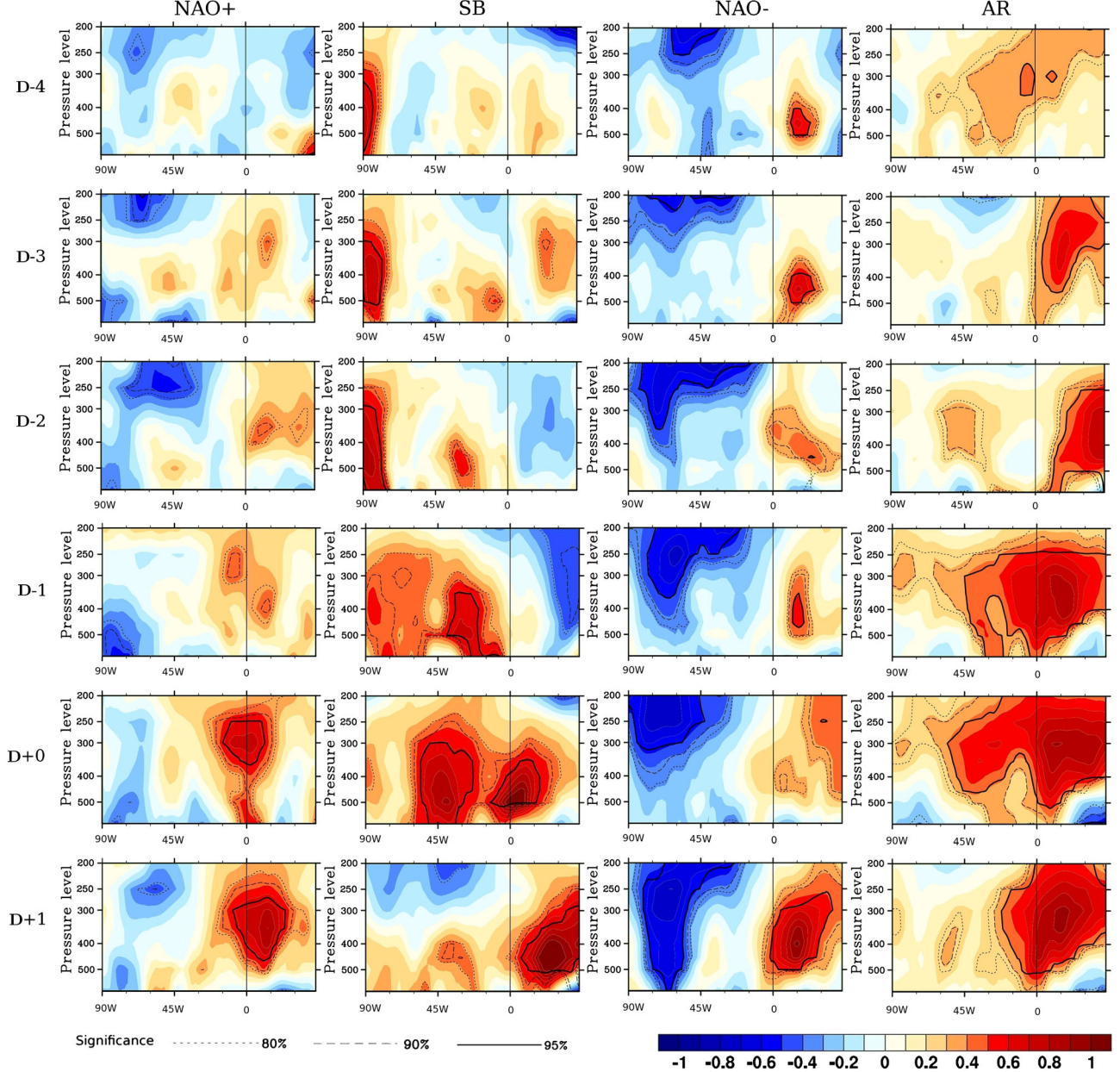


Figure 15. Evolution of vertical (from 600 to 200 hPa) PV standardized anomalies from 4 days before the key day to 1 day after. The west-east cross sections at latitude 71.25°N are centered on the longitude of the PL formation position. The cold season period considered is November 2000 to March 2011. The significant levels are indicated by solid and dotted lines.

[48] This study corroborates the suggestion of a continuum of PLs over this area [Rasmussen and Turner, 2003]. Concerning specifically the Labrador Sea, our results confirm to a large extent the intuition of Rasmussen *et al.* [1996] that a large majority of PLs form under similar conditions.

[49] While our results are in line with Blechschmidt *et al.* [2009] and Zahn and von Storch [2008], who used different methods to infer the large-scale environments favorable for PL development, they tend to generalize their results through the use of several lists of observed PLs. Blechschmidt *et al.* (2008) calculated composites based on PL geographical location, while Zahn and von Storch [2008] performed a Canonical Correlation Analysis of mean

sea level pressure maps from a local climate model and PLs detected through dynamical downscaling of NCEP/NCAR reanalyses. The major mode found by these authors to be favorable for PL development corresponds to the AR regime. The use of a WR paradigm accounting for the non-orthogonality of the circulation modes, their spatial asymmetry, and other properties, as well as the timescale interaction between small-scale and short lifetime phenomena like PLs and stationary waves alteration, helps better document the overall dynamics of PLs. Finally, our study emphasizes the need to build long and consistent inventories of PLs to permit stronger statistics useful for improving forecasts.

[50] **Acknowledgments.** The authors thank B. Duchiron for preliminary results which inspired the present work. ERA-I and NCEP/NCAR data were obtained through CLIMSERV. We thank G. W. K. Moore and two anonymous reviewers for their comments on an earlier version of the manuscript. We acknowledge A. M. Carleton for reading the revised manuscript.

References

- Anderberg, M. R. (1973), Cluster Analysis for Applications, 359 pp., Academic Press, New York.
- Auer, Jr. A. H. (1986), An observational study of polar air depressions in the Australian region, in Preprint Volume, Second International Conference on Southern Hemisphere Meteorology, December 1–5, 1986, pp. 46–49, Amer. Met. Soc., Boston, Mass.
- Blackmon, M. L., Y. H. Lee, and J. M. Wallace (1984), Horizontal structure of 500mb height fluctuations with long, intermediate and short time scales, *J. Atmos. Sci.*, **41**, 961–979.
- Blechschmidt, A.-M., S. Bakan, and H. Graßl (2009), Large-scale atmospheric circulation patterns during polar low events over the Nordic seas, *J. Geophys. Res.*, **114**, D06115, doi:10.1029/2008JD010865.
- Bracegirdle, T. J., and S. L. Gray (2008), An objective climatology of the dynamical forcing of polar lows in the Nordic seas, *Int. J. Climatol.*, **28**, 1903–1919, doi:10.1002/joc.1686.
- Businger, S. (1985), The synoptic climatology of polar low outbreaks, *Tellus*, *Ser. A*, **37**, 419–432.
- Businger, S. (1987), The synoptic climatology of polar-low outbreaks over the Gulf of Alaska and the Bering Sea, *Tellus*, *Ser. A*, **39**, 307–325.
- Businger, S., and J. J. Baik (1991), An arctic hurricane over the Bering Sea, *Mon. Wea. Rev.*, **119**, 2293–2322.
- Carleton, A. M., D. Carpenter (1990), Satellite climatology of “polar low” and broadscale climatic associations for the southern hemisphere, *Int. J. Climatol.*, **10**, 219–246.
- Cassou, C. (2008), Intraseasonal interaction between the Madden-Julian Oscillation and the North Atlantic Oscillation, *Nature*, doi:10.1038/nature07286.
- Cassou, C., M. Minvielle, L. Terray, and C. Périgaud (2011), A statistical-dynamical scheme for reconstructing ocean forcing in the Atlantic. Part I: Weather regimes as predictors for ocean surface variables, *Clim. Dyn.*, doi:10.1007/s00382-010-0781-7.
- Cavalieri, D., C. Parkinson, P. Gloersen, and H. J. Zwally (1996), Sea Ice Concentrations from Nimbus-7 SMMR and DMSP SSM/I-SSMIS Passive Microwave Data, (1979–2007), National Snow and Ice Data Center, Digital media: Boulder, Colorado USA.
- Claud, C., A. M. Carleton, B. Duchiron, and P. Terray (2009a), Southern hemisphere winter cold-air mesocyclones: Climatic environments and associations with teleconnections, *Clim. Dyn.*, **33**, 383–408, doi:10.1007/s00382-008-0468-5.
- Claud, C., A. M. Carleton, B. Duchiron, and P. Terray (2009b), Atmospheric and upper ocean environments of Southern polar mesocyclones in the transition season months and associations with teleconnections, *J. Geophys. Res.*, **114**, D23104, doi:10.1029/2009JD011995.
- Claud, C., B. Duchiron, and P. Terray (2007), Associations between large-scale atmospheric circulation and polar low developments over the North Atlantic during winter, *J. Geophys. Res.*, **112**, D12101, doi:10.1029/2006JD008251.
- Claud, C., Heinemann G., Raastein E., and L. McMurdie (2004), Polar low *le Cygne*, Satellite observations and numerical simulations, *Q. J. R. Meteorol. Soc.*, **130**, 1075–1102.
- Claud, C., N. M. Mognard, K. B. Katsaros, A. Chedin, and N. A. Scott (1993), Satellite observations of a polar low over the Norwegian Sea by Special Sensor Microwave/Imager, Geosat and TIROS-N Operational Vertical Sounder, *J. Geophys. Res.*, **98**, 14487–14506.
- Condron, A., I. A. Renfrew (2013), The impact of polar mesoscale storms on northeast Atlantic Ocean circulation, *Nat. Geosci.*, **6**, 34–37, doi:10.1038/NGEO1661.
- Condron, A., G. R. Bigg, and I. A. Renfrew (2006), Polar mesocyclones in the northeast Atlantic: Comparing climatologies from ERA-40 and satellite imagery, *Mon. Weather Rev.*, **134**, 1518–1533.
- Davison A. C., and D. V. Hinkey (1997), Bootstrap Methods and Their Application, 582 pp, Cambridge Univ. Press, New York.
- Dee D. P., et al. (2011), The ERA-Interim reanalysis: Configuration and performance of the data assimilation system. *Q. J. R. Meteorol. Soc.*, **137**, 553–597, doi:10.1002/qj.828.
- van Delden, A., E. A. Rasmussen, J. Turner, and B. Røsting (2003), Theoretical investigations, in *Polar Lows*, edited by E. A. Rasmussen and J. Turner. Cambridge Univ. Press, Cambridge, U.K.
- Douglas M., L. S. Fedor, and M. A. Shapiro (1991), Polar low structure over the northern Gulf of Alaska based on research aircraft observations, *Mon. Weather Rev.*, **119**, 32–54.
- Doyle, J., and M. A. Shapiro (1999), Flow response to large-scale topography: The Greenland tip jet, *Tellus*, *Ser. A*, **51**, 728–748.
- Ese, T., I. Kanestrom, and K. Pedersen (1988), Climatology of polar lows over the Norwegian and Barents Seas, *Tellus*, *Ser. A*, **40**, 248–255.
- Feldstein, S. B. (2000), The timescale, power spectra and climate noise properties of teleconnection patterns, *J. Climate*, **13**, 4430–4440.
- Forbes, G. S., and W. D. Lottes (1985), Classification of mesoscale vortices in polar airstreams and the influence of the large-scale environment on their evolution, *Tellus*, *Ser. A*, **37**, 132–155.
- Ghil M., and A. W. Robertson (2002), Waves vs Particles in the atmospheric phase space: A pathway to long-range forecasting? *Proc. Natl. Acad. Sci. USA*, **99**, 2493–2500.
- Harrold, T. W., and K. A. Browning (1969), The polar low as a baroclinic disturbance, *Q. J. R. Meteorol. Soc.*, **95**, 710–723.
- Heinemann, G., and C. Claud (1997), Report of a workshop on “Theoretical and observational studies of polar lows” of the European Geophysical Society Polar Lows Working Group, *Bull. Am. Met. Soc.*, **78**, 2643–2658.
- Hewson, T. D., G. C. Craig, and C. Claud (2000), Evolution and mesoscale structure of a polar low outbreak, *Q. J. R. Meteorol. Soc.*, **126** (A), 1031–1063.
- Hoskins, B. J., M. E. McIntyre, A. W. Robertson (1985), On the use and significance of isentropic potential vorticity maps, *Q. J. R. Meteorol. Soc.*, **111**, 877–946.
- Inoue, J., M. E. Hori, Y. Tachibana, and T. Kikuchi (2010), A polar low embedded in a blocking high over the Pacific Arctic, *Geophys. Res. Lett.*, **37**, L14808, doi:10.1029/2010GL043946.
- Kalnay, E., et al. (1996), The NCEP/NCAR 40-Year Reanalysis Project, *Bull. Amer. Meteor. Soc.*, **77**, No. 3, 437–470.
- Kolstad, E. W. (2011), A global climatology of favourable conditions for polar lows, *Q. J. R. Meteorol. Soc.*, doi:10.1002/qj.888.
- McMurdie, L. A., C. Claud, and S. Atakurt (1997), Satellite-derived characteristics of spiral and comma-shaped southern hemisphere mesocyclones, *J. Geophys. Res.*, **102**, 13889–13905.
- Michelangeli P., R. Vautard, B. Legras (1995), Weather regimes: Recurrence and quasi stationarity, *J. Atmos. Sci.*, **52**, 1237–1256.
- Minik, L. M., I. A. Gurvich, and M. K. Pichugin (2011), Satellite sensing of intense winter mesocyclones over the Japan Sea, *IEEE International Geoscience and Remote Sensing Symposium (IGARSS)*, 2345–2348.
- Montgomery, M. T., and D. F. Farrell (1992), Polar low dynamics, *J. Atmos. Sci.*, **49**, 2484–2505.
- Moore, G. W. K., M. C. Reader, J. York, and S. Sathyamoorthy (1996), Polar lows in the Labrador Sea—A case study, *Tellus*, *Ser. A*, **48**, 17–40.
- Ninomiya, K. (1989), Polar/comma-cloud lows over Japan Sea and the Northwestern Pacific, *J. Meteor. Soc. Japan*, **67**, 83–97.
- Ninomiya, K., K. Hoshino, and K. Kurihara, (1990), Evolution process and multi-scale structure of a polar low developed over the Japan Sea on 11–12 December 1985, *J. Meteor. Soc. Japan*, **68**, 293–306.
- Noer, G., and M. Ovhed (2003), Forecasting of polar lows in the Norwegian and the Barents Sea, Paper Presented at the 9th Meeting of the EGS Polar Lows Working Group, Eur. Geophys. Soc., Cambridge, U. K.
- Noer, G., Ø. Saetra, T. Lien, and Y. Guddal (2011), A climatological study of polar lows in the Nordic Seas. *Q. J. R. Meteorol. Soc.*, doi:10.1002/qj.846.
- Parker, M. N. (1989), Polar lows in the Beaufort Sea, in *Polar and Arctic Lows*, edited by P.F. Twitchell, E. A. Rasmussen and K. L. Davidson, pp. 420, A. Deepack, Hampton, Va.
- Parker, M. N. (1997), *Cold Air Vortices and Polar Low Handbook for Canadian Meteorologists*, Environ. Canada, Edmonton, Can.
- Rasmussen, E. A. (1990), On the application of satellite data for forecasting/nowcasting and research of polar lows, Preprint Volum of the Fifth Conference on Satellite Meteorology and Oceanography, September 3–7, London, England.
- Rasmussen, E. A. and J. Turner (2003), *Polar Lows: Mesoscale Weather Systems in the Polar Regions*, Cambridge Univ. Press, New York.
- Rasmussen, E. A., C. Claud, and J. F. Purdon (1996), Labrador Sea polar lows, *Global Atmos-Ocean Syst.*, **4**, 275–333.
- Rasmussen, E. A., J. Turner, and P. F. Twitchell (1993), Report of a workshop on applications of new forms of satellite data in polar low research, held at Hvanneyri, Iceland, 23–26 June 1992, *Bull. Amer. Meteor. Soc.*, **74**, 1057–1073.
- Saetra, Ø., T. Linders, and J. B. Debernard (2008), Can polar lows lead to warming of the ocean surface?, *Tellus*, *Ser. A*, **60**, 141–153.
- Sanchez-Gomez, E., L. Terray, and B. Joly (2008), Intra-seasonal atmospheric variability and extreme precipitation events in the European-Mediterranean region, *Geophys. Res. Lett.*, **35**, L15708, doi:10.1029/2008GL034515.
- von Storch, H., and F. Zwiers (1999), *Statistical Analysis in Climate Research*, 494 pp, Cambridge Univ. Press, New York.

- Straus, D. M., S. Corti, F. Molteni (2007), Circulation regimes: Chaotic variability versus SST-Forced predictability, *J. Clim.*, 20, 2251–2272.
- Vautard, R. (1990), Multiple weather regimes over the North Atlantic: Analysis of precursors and successors, *Mon. Wea. Rev.*, 118, 2056–2081.
- Wallace, J. M., and D. Gutzler (1981), Teleconnections in the geopotential fields during the Northern Hemisphere winter, *Mon. Wea. Rev.*, 109, 784–812.
- Wilhelmsen, K. (1985), Climatological study of gale-producing polar lows near Norway, *Tellus, Ser. A*, 37, 451–459.
- Yanase, W., G. Fu, H. Niino, and T. Kato (2004), A Polar Low over the Japan Sea on 21 January 1997. Part II: A Numerical Study, *Mon. Wea. Rev.*, 132, 1552–1574.
- Zahn, M., and H. von Storch (2008), A long-term climatology of North Atlantic polar lows, *Geophys. Res. Lett.*, 35, L22702, doi:10.1029/2008GL035769.
- Zick, C. (1994), Polar lows in the SW Pacific region and their transition from or into synoptic-scale cyclones, in The Life Cycles of Extratropical Cyclones, Proceeding of an International Symposium, 27 June–1 July, 1994, University of Bergen, Norway, Volume III ed. S. Grønas, M. A. Shapiro, 248–255 pp., American Meteorological Society, Boston.